Electronic Supplementary Material (ESI) for CrystEngComm.

Supporting Information

Catalyst preparation

A certain of aqueous $NiCl_2 \cdot 6H_2O$ (20 mM), $H_2PtCl_6 \cdot 6H_2O$ (20 mM), KI (5 M), EG, and deionized water were added in a 25-mL bottle and stirred for 30 min to form a homogeneous solution. Then the obtained solution was transferred into an autoclave and heated at 200 °C for 6 h, and cooled to room temperature. The obtained samples were collected by centrifugation at 10,000 rpm for 10 min, and then washed with ethanol and deionized water for several times.

The experimental parameters were adjusted as follows (Table S1-Table S6).

Sample	$NiCl_2 \cdot 6H_2O$ /mL	$H_2PtCl_6 \cdot 6H_2O$ /mL	PVP /mg	KI /mL	H_2O /mL	EG /mL
1	0	1.2	220	0.04	6.4	1.6
2	0.1	1.2	220	0.04	6.4	1.6
3	0.4	1.2	220	0.04	6.4	1.6
4	2	1.2	220	0.04	6.4	1.6
5	5	1.2	220	0.04	6.4	1.6
6	6.5	1.2	220	0.04	6.4	1.6
7	8.0	1.2	220	0.04	6.4	1.6
8	10	1.2	220	0.04	6.4	1.6

Sample	$NiCl_2 \cdot 6H_2O$ /mL	$H_2PtCl_6 \cdot 6H_2O$ /mL	PVP /mg	KI /mL	H_2O /mL	EG /mL
1	0.4	1.2	220	0.04	0	8
2	0.4	1.2	220	0.04	0.8	7.2
3	0.4	1.2	220	0.04	3.2	4.8
4	0.4	1.2	220	0.04	5.6	2.4
5	0.4	1.2	220	0.04	6.4	1.6

Sample	$MCl_x\cdot yH_2O$ /mL	$H_2PtCl_6\cdot 6H_2O$ /mL	PVP /mg	KI /mL	H_2O /mL	EG /mL
Pt-Ni-N NFs	0.4	1.2	220	0.04	6.4	1.6
Pt-Fe-N	0.4	1.2	220	0.04	6.4	1.6
Pt-Co-N	0.4	1.2	220	0.04	6.4	1.6
Pt-Cu-N	0.4	1.2	220	0.04	6.4	1.6
Pt-Mn-N	0.4	1.2	220	0.04	6.4	1.6

Sample	$NiCl_2\cdot 6H_2O$ /mL	$H_2PtCl_6\cdot 6H_2O$ /mL	PVP /mg	KI /mL	H_2O /mL	EG /mL	Time/ min
1	0.4	1.2	220	0.04	6.4	1.6	10
2	0.4	1.2	220	0.04	6.4	1.6	30
3	0.4	1.2	220	0.04	6.4	1.6	120
4	0.4	1.2	220	0.04	6.4	1.6	240
5	0.4	1.2	220	0.04	6.4	1.6	360
6	0.4	1.2	220	0.04	6.4	1.6	480

Sample	$NiCl_2\cdot 6H_2O$ /mL	$H_2PtCl_6\cdot 6H_2O$ /mL	PVP /mg	KI /mL	H_2O /mL	EG /mL
1	0.4	1.2	220	0.02	6.4	1.6
2	0.4	1.2	220	0.04	6.4	1.6
3	0.4	1.2	220	0.08	6.4	1.6
4	0.4	1.2	220	0.16	6.4	1.6
5	0.4	1.2	220	0.20	6.4	1.6

Sample	$NiCl_2\cdot 6H_2O$ /mL	$H_2PtCl_6\cdot 6H_2O$ /mL	PVP /mg	KI /mL	H_2O /mL	EG /mL
Pt-Ni-N NFs	0.4	1.2	220	0.04	6.4	1.6
Pt-Ni-N NPs	10	1.2	220	0.04	6.4	1.6
Pt-Ni	0.4	1.2	--	0.04	6.4	1.6
Pt-N	--	1.2	220	0.04	6.4	1.6

DFT method

DFT calculations were performed using the CASTEP model in the Materials Studio with optimized calculating parameters. Geometry optimization of the Pt-Ni-N is converged when force was below 0.03 eV/Å. The Pt-Ni-N (111) surface and (220) surface models were sliced with three-layer slab separated by a 15 Å of vacuum region with the two frozen bottom layers. The adsorption and reaction calculations were carried out on 2x2 surface unit cells. All the small molecules (CH_3OH CO H_2O) and free radicals (CH_3O H CHO CH_2O) adsorption models were optimized to be stable state. The tolerances of energy, force, and displacement convergence in atomic relaxation sections were 1×10^{-5} eV/atom, 3×10^{-2} eV/Å, and 1×10^{-3} Å, respectively. All the nonperiodical structures include small molecules and free radicals were optimized in an empty crystal lattice with the parameter of a=b=c= 25 Å. The energies were calculated under the same condition after optimization. A LST/QST method with RMS convergence of 0.05 eV/ Å was utilized to search transition state (TS). The adsorption energy was calculated as follows:

$$E_{ads}= E_{adsorbate} + E_{M} - E_{adsorbate/M}$$

where E_{ads}, $E_{adsorbate}$, E_M and $E_{adsorbate/M}$ represents the adsorption energies on the alloy surfaces, free adsorbate, pure alloy surfaces and adsorption system models, respectively. For a particular reaction, the reaction energy (ΔH) and activation barrier (Ea) were calculated by the following equations:

$$\Delta H = E_{(A+B)/M} - E_{AB/M}$$

$$E_a = E_{TS/M} - E_{AB/M}$$

Catalyst evaluation

Typically, a glassy carbon electrode or glassy carbon rotating disk electrode with diameter of 3 mm was polished with 0.05 μm α-Al_2O_3 powder before the modification, and then ultrasonically washed by ethanol and deionized water. Then, 5 mg of catalyst was added in 375 uL of deionized water, 125 uL of absolute ethanol and 25 uL of Nafion® (5%). And 0.002 mL ink was dispersed onto the GCE surface and dried at room temperature.

Methanol oxidation reaction (MOR)

Voltammetric measurements were performed on a CHI 760E electrochemical workstation. Pt wire and Ag/AgCl were used as counter electrode and reference electrode, respectively. A modified GCE was used as the working electrode. The scans range from -0.2 to 1.0 V in the nitrogen saturated 0.5 M H_2SO_4 solution (25 °C) repeated several times until a stable curve was observed. CVs for MOR were carried out in 0.5 M H_2SO_4 and 1.0 M methanol. The current density–time (i–t) curves were obtained at a fixed potential in 0.5 M H_2SO_4 and 1.0 M CH_3OH.

Oxygen reduction reaction (ORR)

For ORR measurements, the polarization curves were recorded by applying a linear potential scan ranging from 400 to 2400 rpm. Pt wire and Ag/AgCl were used as the counter electrode and reference electrode, respectively. The slopes of the linear fitting lines were used to estimate the number of electrons (n) according to the Koutecky–Levich equation:

$$\frac{1}{j}=\frac{1}{j_k}+\frac{1}{j_d}=\frac{1}{j_k}+\frac{1}{B\varpi^{1/2}}$$

$$B=0.62nFC_0{D_0}^{2/3}\nu^{-1/6}$$

where j, j_k and j_d represent the measured, the kinetic and the diffusion-limiting current, respectively, w is the rotating speed, v is the kinetic viscosity of the electrolyte (1.009×10^{-2}

$cm^2 \cdot s^{-1}$), D_0 is the oxygen diffusivity (1.1×10^{-5} $cm^2 \cdot s^{-1}$), C_0 is the oxygen solubility (1.6×10^{-3} $mol \cdot L^{-1}$), F is the Faraday constant, and n is the number of electrons. The stability test was performed in 0.1 M $HClO_4$ for 1000 cycles.

Figure S1

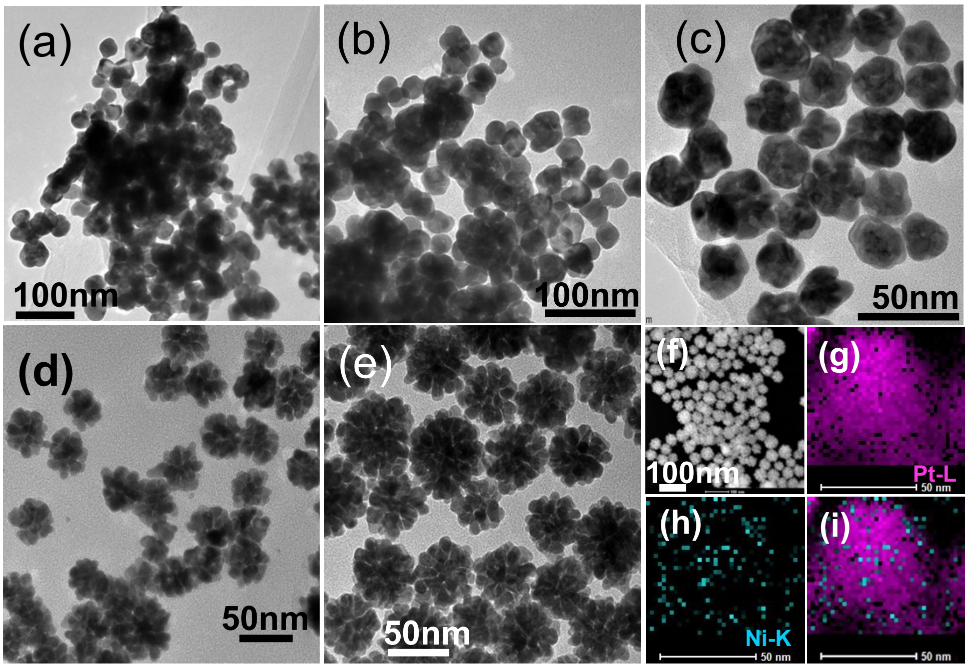

Figure S1. TEM, HAADF-STEM images, and the corresponding mapping results of Pt, Ni and N in typical Pt-Ni-N nanoflowers prepared with different volume ratios of water to EG: (a) 0:8, (b) 1:9, (c) 2:3, (d) 7:3 and (e)-(i) 4:1.

Figure S2

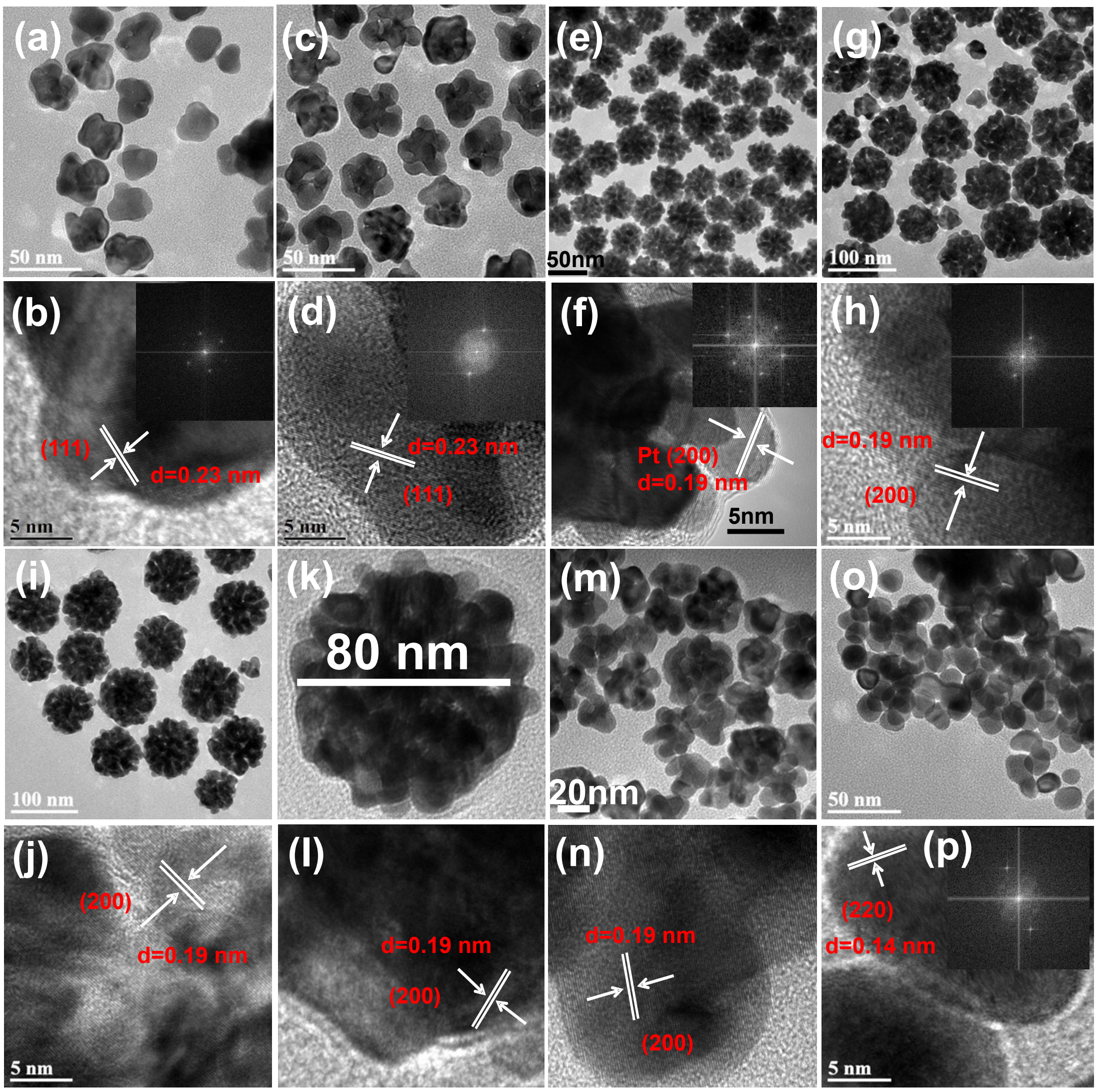

Figure S2. TEM and HR-TEM images of the Pt-Ni-N nanocatalysts prepared with different volumes of Ni^{2+}: (a-b) 0 mL, (c-d) 0.1 mL, (e-f) 0.4 mL, (g-h) 2 mL, (i-j) 5 mL, (k-l) 6.5 mL, (m-n) 8.0 mL , and (o-p) 10 mL.

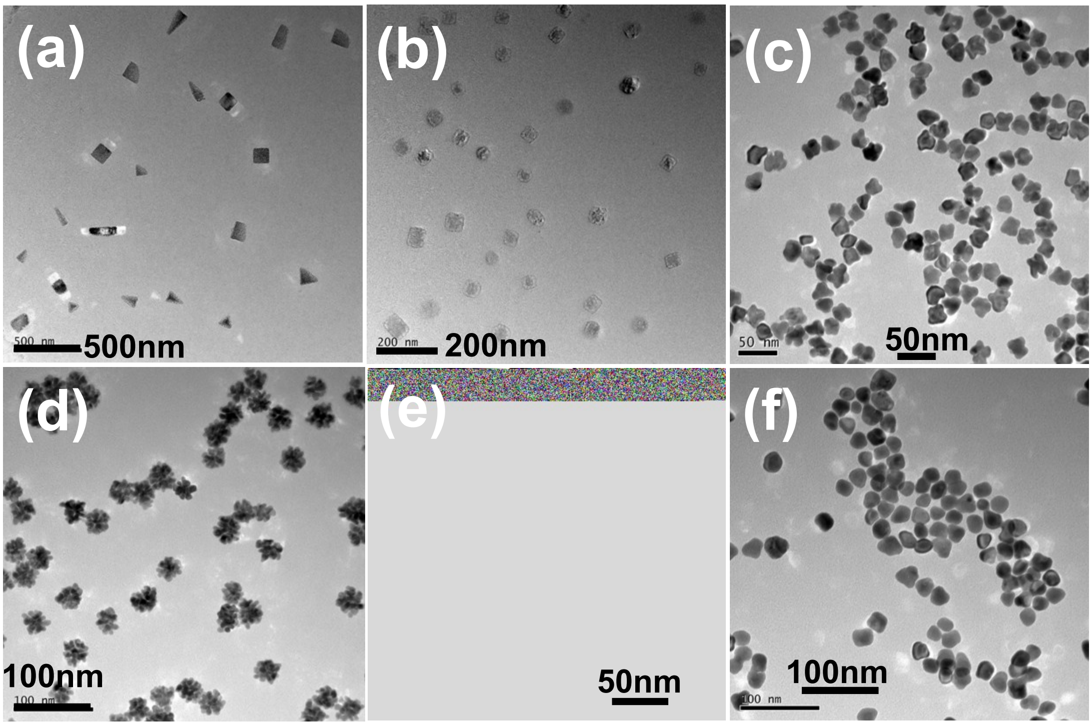

Figure S3. TEM images of Pt-Ni-N obtained with different reaction durations: (a) 10 min; (b) 30 min; (c) 120 min; (d) 240 min; (e) 360 min; and (f) 480 min.

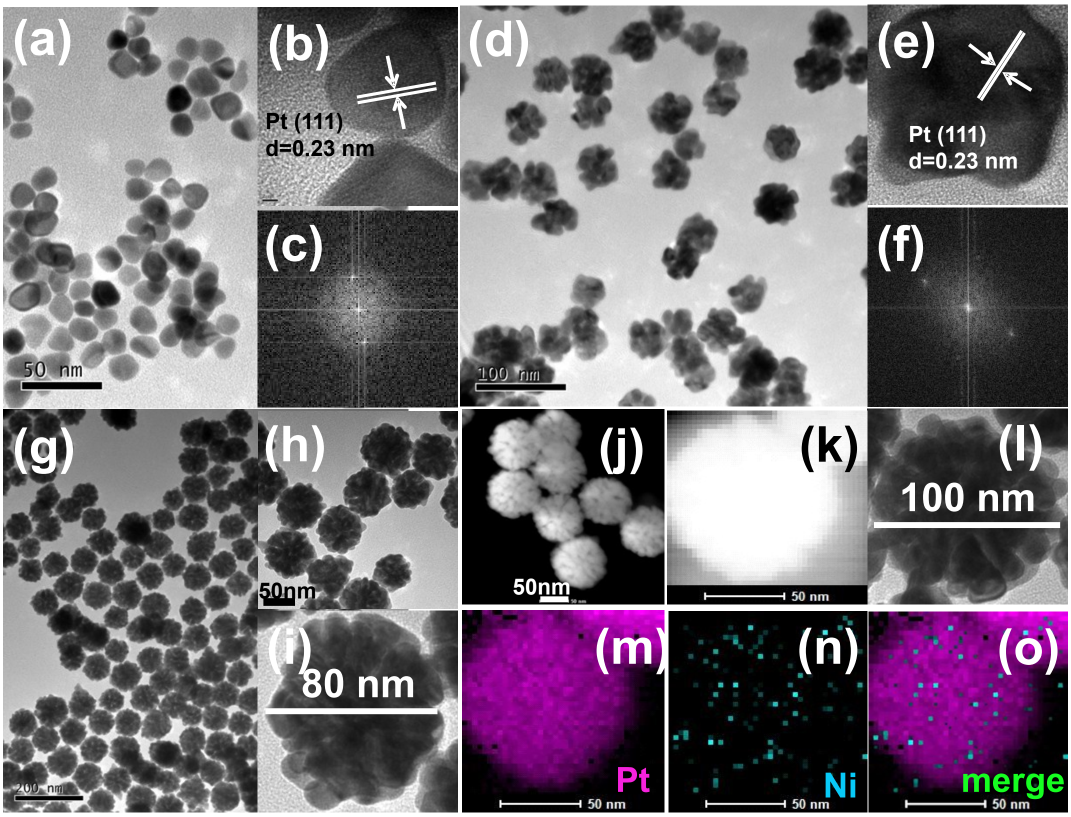

Figure S4. TEM, HRTEM and HAADF-STEM images and the corresponding mapping results in typical Pt-Ni-N catalysts obtained through the addition of different amounts of KI aqueous solution in the synthesis while keeping the other parameters constant: (a-c) 20 μL, (d-f) 80 μL, (g-i) 160 μL, (j-o) 200 μL.

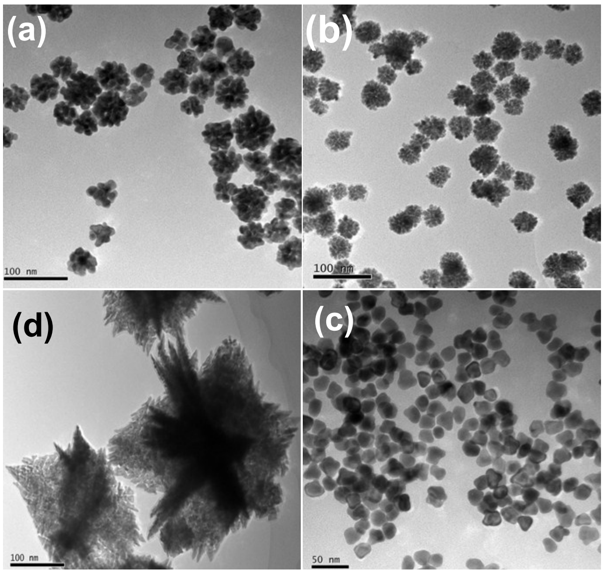

Figure S5. TEM images of PtMN nanoflowers obtained through the addition of different kinds of M^{2+} in the synthesis while keeping the other parameters constant: (a) Pt-Fe-N; (b) Pt-Co-N; (c) Pt-Cu-N; and (d) Pt-Mn-N.

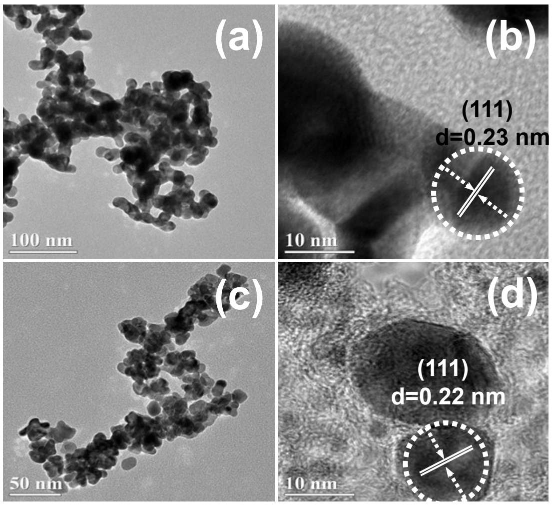

Figure S6. TEM images of (a) (b) PtNi and (c) (d) PtN NPs.

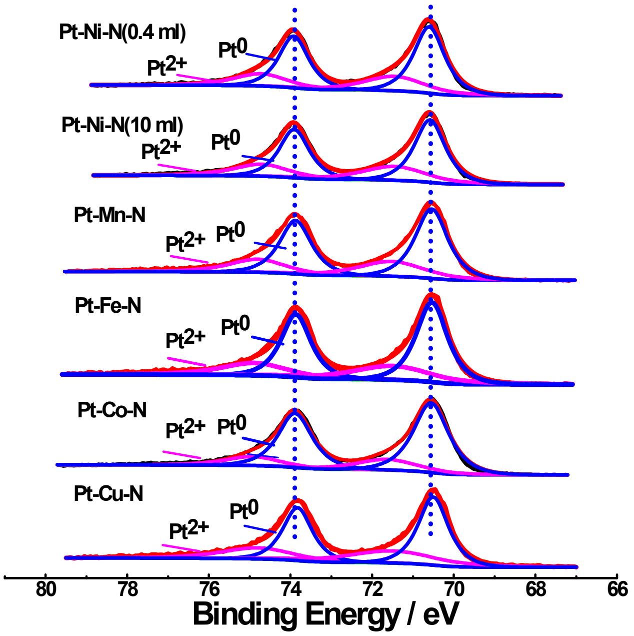

Figure S7. XPS spectra of Pt 4f for the Pt-M-N nanoparticles, Pt-N and Pt-Ni catalysts.

The binding energy (BE) values at 74.6 and 71.3 eV correspond to Pt $4f_{5/2}$ and Pt $4f_{7/2}$, respectively, which can be assigned to Pt^0 species for Pt-M-N catalyst. And two more peaks at 75.8 and 72.2 eV indicate the presence of Pt^{2+} species. According to Pt^0/Pt^{2+} intensity ratio, the element Pt in Pt-M-N nanocatalyst is predominantly in the zero-valent state (~65%-70.2%).

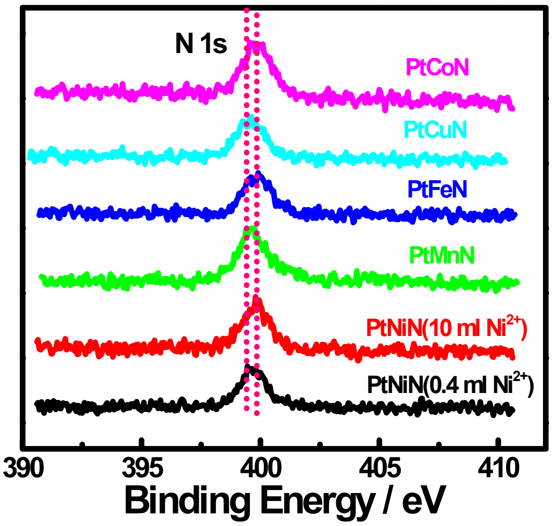

Figure S8. XPS spectra of N 1s for the Pt-M-N nanoparticles, Pt-N and Pt-Ni catalysts.

Furthermore, 2.4-6.54 wt % nitrogen was estimated to be present in these Pt-M-N hybrids on the basis of the XPS analysis. The high-resolution N 1s scan indicated the presence of pyrrolic N (399.6 ± 0.1 eV), which derived from the surfactant PVP, have been shown to serve as catalytically active sites for MOR and ORR, and no obvious shift has been occurred.

(a) $CH_3OH \rightarrow CH_3O + H$

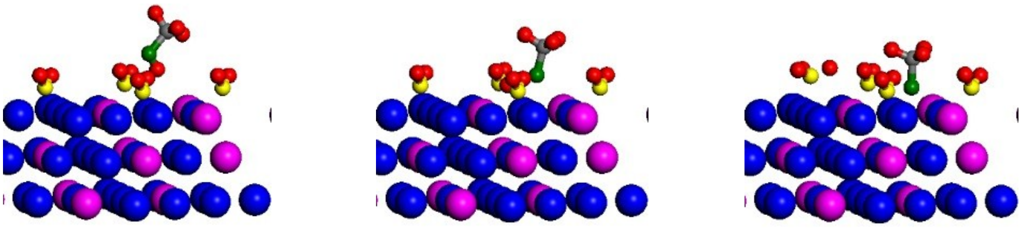

$[CH_3OH]$ (-4.9) TS1 (-3.29) $[CH_3O + H]$ (-11.0)

(b) $CH_3O \rightarrow CH_2O + H$

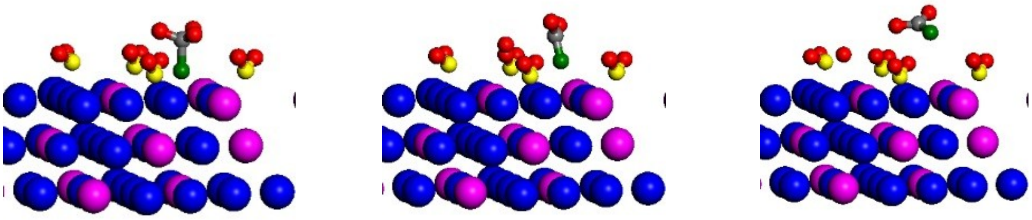

$[CH_3O]$ (-6.4) TS2 (-3.5) $[CH_2O + H]$ (-8.8)

(c) $CH_2O \rightarrow CHO + H$

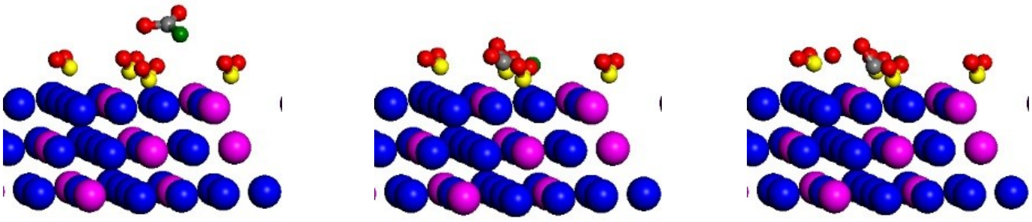

$[CH_2O]$ (-4.1) TS3(-3.7) [CHO + H] (-10.9)

(d) CHO → CO + H

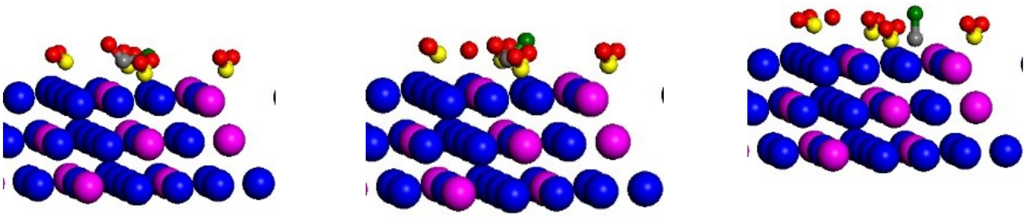

[CHO] (-6.4) TS4 (-5.5) [CO + H] (-10.6)

Figure S9. Dehydrogenation of methanol via initial O-H bond scission on Pt-Ni-N (111). Energies (eV) of the initial, transition, and final states are relative to gas-phase methanol plus the clean slab (with zero-point energy corrections). [A + H] denotes the coadsorbed A and H species.

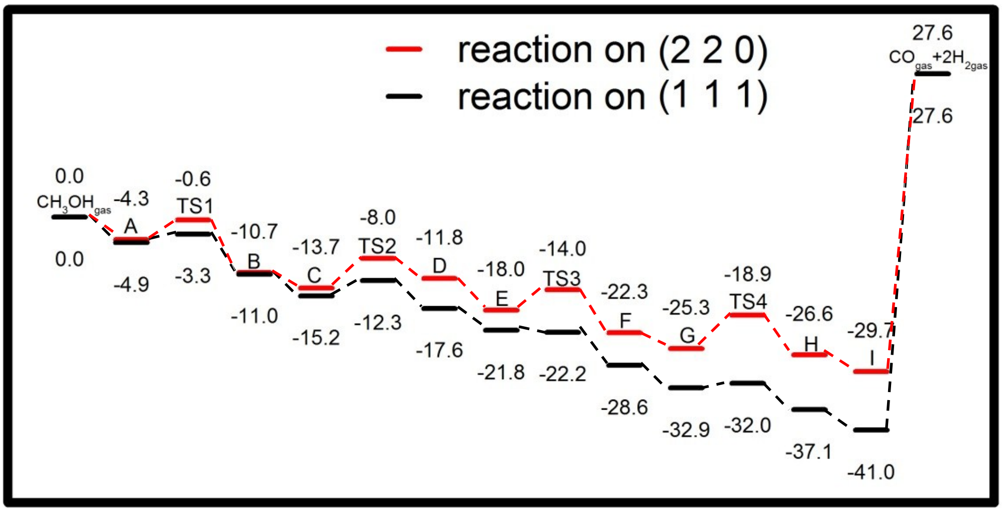

Figure S10. Potential energy surface of methanol dehydrogenation on PtNiN (111) and (220) facets. Energies (eV) are relative to gas-phase methanol plus the clean slab with zero-point energy corrections: A, [CH_3OH]; B, [CH_3O+H]; C, [CH_3O] + [H]; D, [CH_2O + H] + [H]; E, [CH_2O] + 2[H]; F, [CHO+H] + 2[H]; G, [CHO] +3 [H]; H, [CO + H] +3 [H]; I, [CO] + 4[H]. M + n [H] represents adsorptions of M and n H atoms on (n+1) separated slabs.

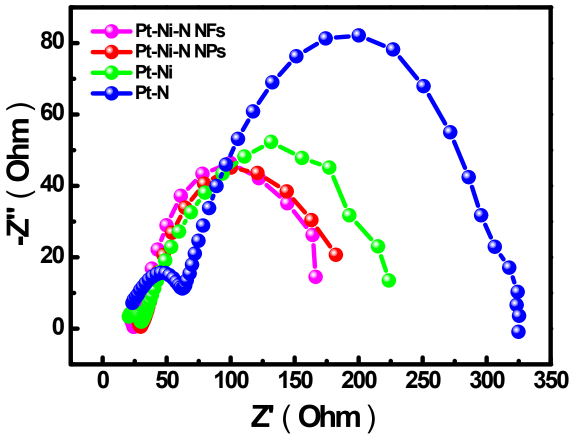

Figure S11. Electrochemical impedance spectroscopy for various Pt-based catalysts measured in N_2-saturated 0.1 M H_2SO_4.

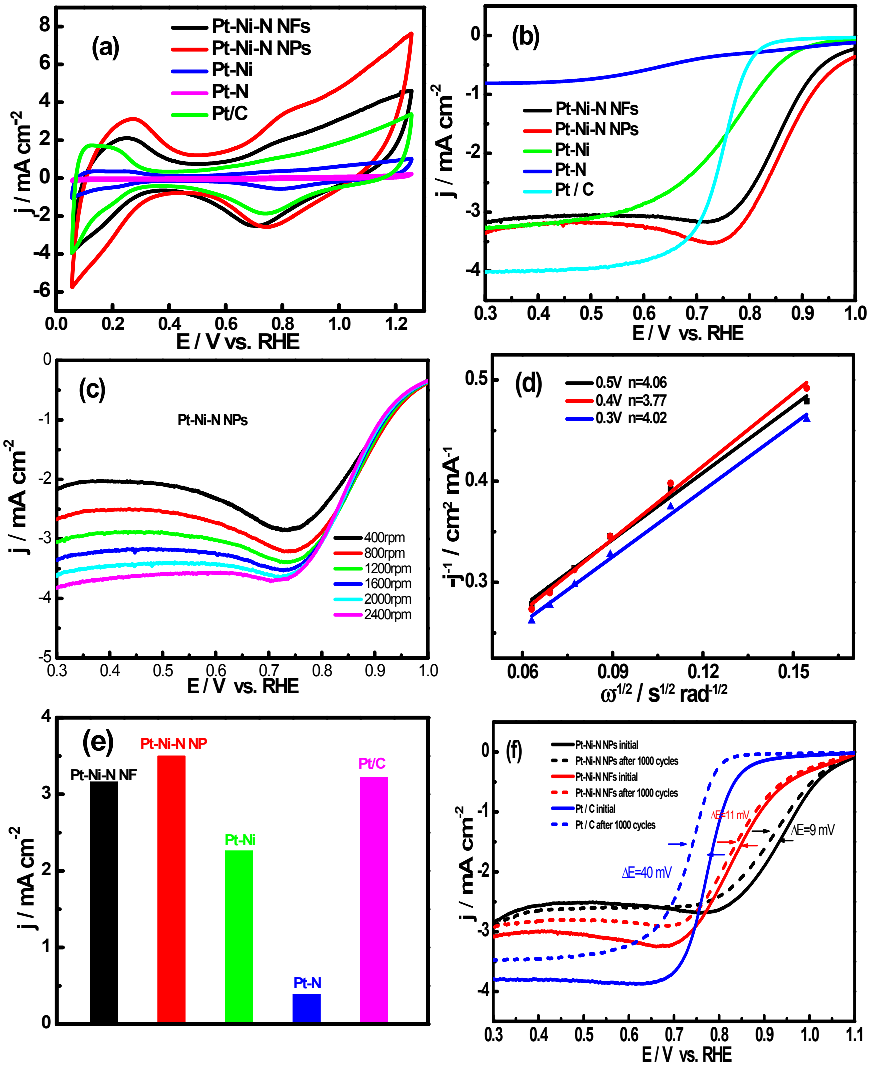

Figure S12 ORR property of Pt-Ni-N NFs, Pt-Ni-N NPs, Pt-Ni catalysts, Pt-N, and the commercial Pt/C catalysts. (a) CVs recorded at room temperature in a N_2-saturated 0.1 M $HClO_4$ solution. (b) ORR polarization curves recorded at room temperature in an O_2-saturated 0.1 M $HClO_4$ solution with a rotation rate of 1600 rpm. (c) ORR polarization curves of Pt-Ni-N NPs at different rotation rates. (d) K-L plots of the ORR from Pt-Ni-N NPs catalysts. (e) Specific activity for these five catalysts. (f) ORR polarization curves of these catalysts before and after stability test of 1000 potential scans.

The electrocatalytic activities of these Pt-Ni-N NFs, Pt-Ni-N NPs, Pt-Ni, Pt-N, and the Pt/C catalysts towards oxygen reduction reaction (ORR) were also studied. Cyclic voltammograms (CVs) were obtained in a N_2-saturated 0.1 M $HClO_4$ solution at a sweep rate of 10 mV s^{-1}. Comparing to the commercial Pt/C catalyst, a positive shift for the onset potential was obtained over Pt-Ni-N, which might owing to the decrease of the deposition free energy of Pt-OH* specials caused by the nitrogen-decorating (Fig.S12a). The ECSA of the Pt-Ni-N NFs was estimated to be 66.3 m^2 g^{-1}, which is about 2.8 times larger than the commercial Pt/C (23.8 m^2 g^{-1}). Fig.S12b shows typical ORR polarization curves for these catalysts obtained in O_2-saturated 0.1 M $HClO_4$

solution. The half-wave potential for Pt-Ni-N NPs is 0.870 V (*vs*. RHE) observed from the Fig. S12b, which is positive than Pt-Ni-N NFs (0.865 V *vs*. RHE), Pt-Ni (0.76 V *vs*. RHE), Pt-N (0.68 V *vs*. RHE), and the commercial Pt/C catalysts (0.73 V *vs*. RHE) (Table S9). The current density indicates the inherent catalytic activity. The specific activities were achieved by normalizing the densities to the ECSA for these catalysts. As revealed in Fig.S12e, the specific activity are 3.2 mA cm^{-2} and 3.5 mA cm^{-2} at 0.7 V (*vs*. RHE) for Pt-Ni-N NFs and Pt-Ni-N NPs, which are 1.4-1.5, 8.2-8.9, and 1.0-1.1 times greater than the Pt-Ni (2.3 mA cm^{-2}), Pt-N (0.39 mA cm^{-2}), and the commercial Pt/C (3.2 mA cm^{-2}), respectively. Clearly, the nitrogen-decorated Pt-Ni-N hybrids exhibit the highest ORR activity among all these catalysts. We can conclude that compared to Pt-Ni, Pt-N, and commercial Pt/C, N-modified process does help to enhance ORR activity to a greater degree.

To calculate the number of transferred electrons (n), the ORR curves were measured in O_2-saturated 0.1 M $HClO_4$ (Figure S12c and Figure S12d). On the basis of the Koutecky-Levich plots (Figure S12d), the n were evaluated to be 3.95 and 3.97 (*vs*. RHE) for Pt-Ni-N NPs and Pt-Ni-N NFs, respectively, revealing the reduction of O_2 *via* a four electron process. The durability is another important issue to be solved for their commercial applications. Thereby, the stability tests were performed in our present study. After 1000 cycles, about 9 and 11 mV negative shifts for the half-wave potentials over Pt-Ni-N NPs and Pt-Ni-N NFs, were observed, while negative shifts of 40 mV was observed for the commercial Pt/C (Figure S12f). It reveals that the Pt-Ni-N catalysts are highly stable under the current ORR environment. To evaluate the number of transferred electrons (n) for these catalysts, the corresponding ORR polarization curves were recorded in O_2-saturated 0.1 M $HClO_4$ at a scan rate of 10 mV s^{-1} with different rotating rates (Figure S13-Figure S14). According to the Koutecky-Levich plots, the n values were calculated to be about 3.9 (*vs*. RHE) for these catalysts, indicating the efficient reduction of O_2 to H_2O *via* a direct four electron pathway

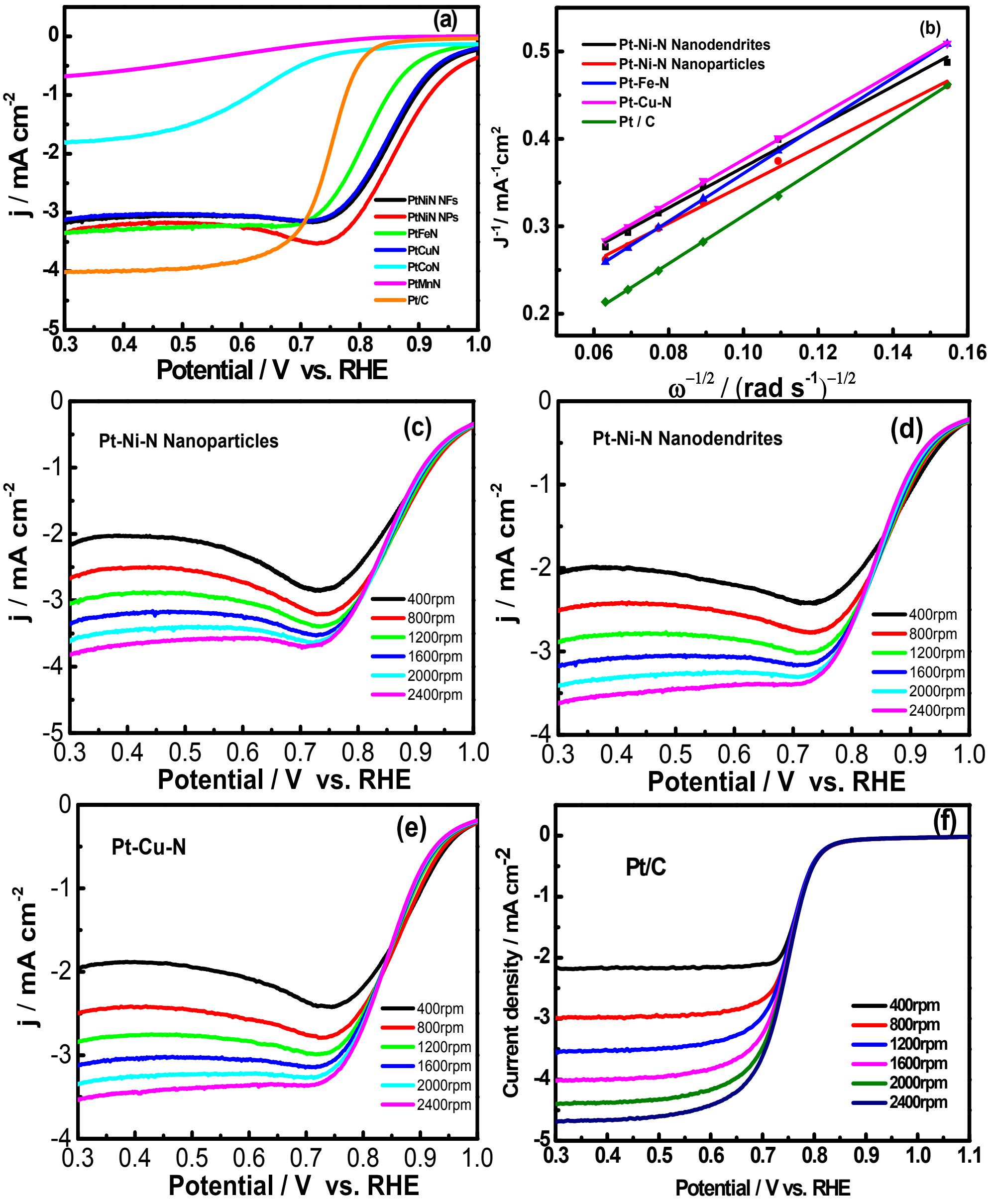

Figure S13. (a) ORR polarization curves from various catalysts recorded at room temperature in an O_2-saturated 0.1 M $HClO_4$ solution with a sweep rate of 10 mV s^{-1} and a rotation rate of 1600 rpm; (b) K-L plots of the ORR from various catalysts; (c-f) ORR polarization curves from various catalysts recorded at different rotation rates.

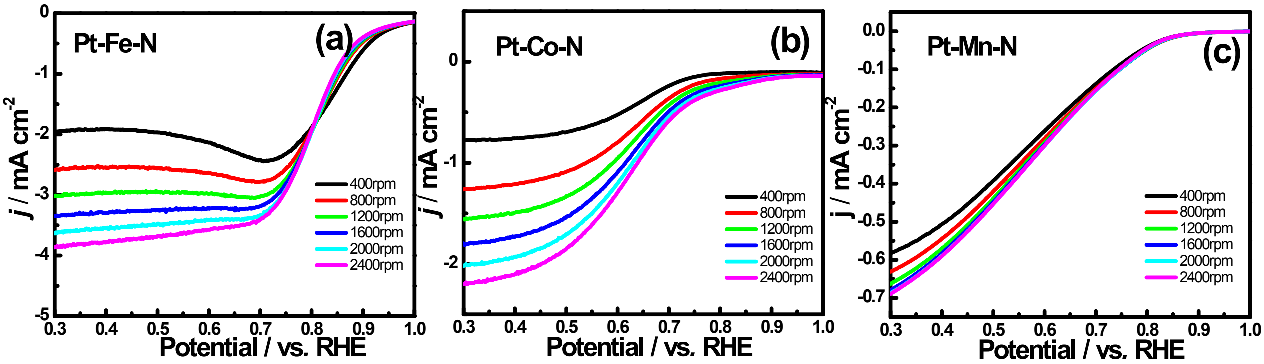

Figure S14. ORR polarization curves from various catalysts recorded at different rotation rates, (a) Pt-Fe-N, (b) Pt-Co-N, and (c) Pt-Mn-N.

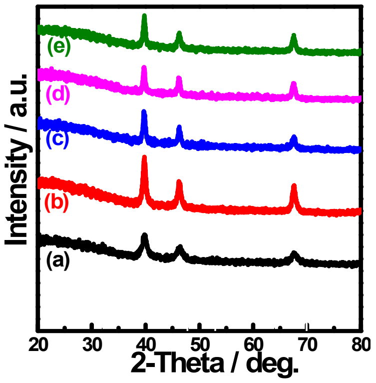

Figure S15. XRD patterns of Pt-Ni-N catalysts obtained through the addition of different amounts of KI aqueous solution in the synthesis while keeping the other parameters constant: (a) 20 µL, (b) 40 µL, (c) 80 µL, (d) 160 µL, and (e) 200 µL.

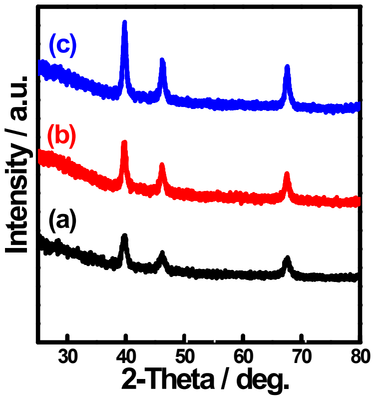

Figure S16. XRD patterns of Pt-Ni-N catalysts prepared with different volume ratios of water to EG: (a) 0:8, (b) 7:3, and (c) 4:1.

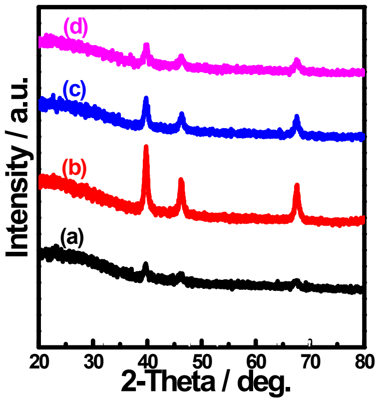

Figure S17. XRD patterns of Pt-Ni-N catalysts prepared with different volumes of Ni^{2+}: (a) 0 mL, (b) 0.4 mL, (c) 5 mL, and (d) 10 mL.

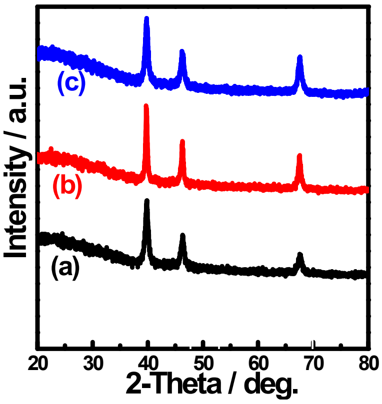

Figure S18. XRD patterns of different catalysts: (a) Pt-Ni, (b) Pt-N, and (c) Pt-Ni-N.

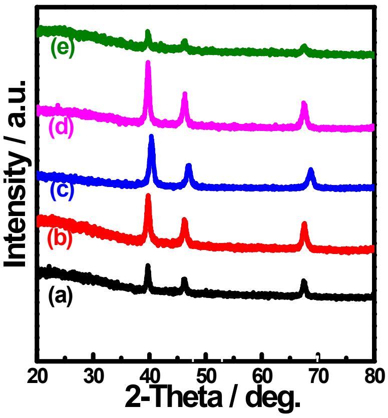

Figure S19. XRD patterns of different catalysts: (a) Pt-Mn-N, (b) Pt-Ni-N, (c) Pt-Co-N, (d) Pt-Cu-N, and (e) Pt-Fe-N.

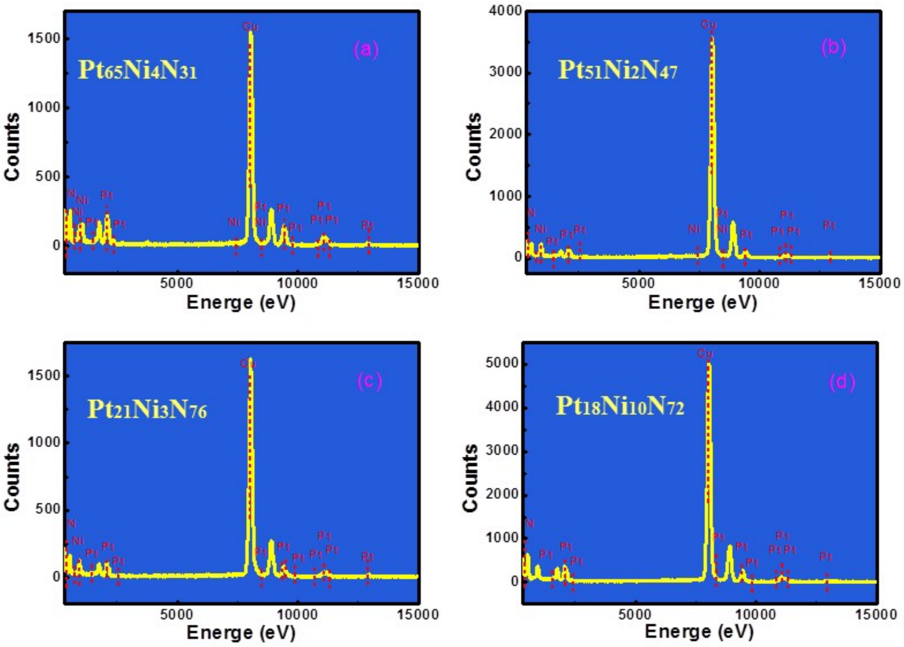

Figure S20. EDX characterization for various Pt-Ni-N catalysts synthesized with different amounts of KI aqueous solution: (a) 20 μL, (d-f) 40 μL, (g-i) 160 μL, (j-o) 200 μL.

Table S7 Catalytic Activities Comparison of Various Catalysts in the Methanol Oxidation Reactions

Catalysts	ECSA ($m^2\ g^{-1}$)	MA(I_f) ($mA\ mg^{-1}$)	MA(I_b) ($mA\ mg^{-1}$)	I_f/I_b	SA(I_f) ($mA\ cm^{-2}$)	SA(I_b) ($mA\ cm^{-2}$)	I_f/I_b
Pt-Ni-N NF	71.5	347.8	246.9	1.41	0.49	0.34	1.44
Pt-Ni-N NP	43.8	177.9	115.6	1.54	0.41	0.26	1.57
Pt-Ni	21.6	122.4	129.4	0.95	0.55	0.58	0.94
Pt-N	12.4	5.52	-	-	0.04	-	-
Pt/C (20%)	28.2	161.3	185.7	0.87	0.55	0.64	0.9

Table S8 Calculated Reaction Energies Δ*H* and Energy Barriers E_a (eV) for All the Elementary Reactions Involved in Methanol Dehydrogenation on PtNiN (111) and (220) facets.

Surface reactions	PtNiN NFs (1 1 1)		PtNiN NPs (2 2 0)	
	Δ*H*	E_a	Δ*H*	E_a
$CH_3OH(g)+M \rightarrow [CH_3OH]$	-4.9	–	-4.3	–
$[CH_3OH] \rightarrow [CH_3O + H]$	-6.1	1.6	-6.4	3.7
$[CH_3O] \rightarrow [CH_2O + H]$	-2.4	2.9	1.9	5.7
$[CH_2O] \rightarrow [CHO + H]$	-6.8	0.4	-4.3	4.0
$[CHO] \rightarrow [CO + H]$	-4.2	0.9	-1.3	6.4
$[CO] \rightarrow CO\ (g) + M$	5.7	–	2.7	–
$[H] \rightarrow 1/2\ H_2\ (g) + M$	8.8	–	6.8	–

Table S9 Half-wave potential ($E_{1/2}$) of the ORR on GC RDEs prepared with five types of nanocatalysts.[a]

Entry	Catalysts	$E_{1/2}$ (V vs. RHE)
1	Pt-Ni-N NFs	0.857
2	Pt-Ni-N NPs	0.860
3	Pt-Mn-N nanoparticle	0.573
4	Pt-Fe-N nanodendrites	0.810
5	Pt-Cu-N trigonal	0.853
6	Pt-Co-N nanodendrites	0.653
7	Pt black	0.690

[a] The polarization curves were recorded in 0.1 M $HClO_4$ with continuous O_2 gas flow at a sweep rate of 10 mVs^{-1} and a rotation speed of 1600 rpm.